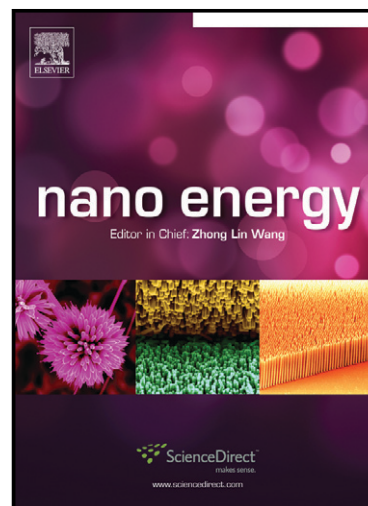# Author's Accepted Manuscript

Cobalt Phosphide Nanorods as an Efficient Electrocatalyst for Hydrogen Evolution Reaction

Zhipeng Huang, Zhongzhong Chen, Zhibo Chen, Cuncai Lv, Mark G. Humphrey, Chi Zhang

nano energy

Editor in Chief: Zhong Lin Wang

ScienceDirect
makes sense.
www.sciencedirect.com

Cite this article as: Zhipeng Huang, Zhongzhong Chen, Zhibo Chen, Cuncai Lv, Mark G. Humphrey, Chi Zhang, Cobalt Phosphide Nanorods as an Efficient Electrocatalyst for Hydrogen Evolution Reaction, *Nano Energy,* http://dx.doi.org/ 10.1016/j.nanoen.2014.08.013

Cobalt Phosphide Nanorods as an Efficient Electrocatalyst for Hydrogen Evolution Reaction

Zhipeng Huang,*[a] Zhongzhong Chen,[a] Zhibo Chen,[a] Cuncai Lv,[a] Mark G. Humphrey,[b] and Chi Zhang*[a]

[a] *China-Australia Joint Research Center for Functional Molecular Materials, Scientific Research Academy, Jiangsu University, Zhenjiang, Jiangsu, P.R. China (212013). Fax/Tel: 86-511-88797815*

[b] *Research School of Chemistry, Australian National University, Canberra, ACT 0200, Australia*

*Corresponding author. Zhipeng Huang, Chi Zhang

E-mail: zphuang@ujs.edu.cn, chizhang@ujs.edu.cn; Phone/Fax: +86-511-88797815

Abstract: Cobalt phosphide (Co_2P) nanorods are found to exhibit efficient catalytic activity in hydrogen evolution reaction (HER), with the overpotential required for the current density of 20 mA/cm^2 as small as 167 mV in acidic solution and 171 mV in basic solution. In addition, the Co_2P nanorods can work stably in both acidic and basic solution during hydrogen production. This performance can be favorably comparable to typical high efficiently non-precious catalysts, and suggest the promising application potential of the Co_2P nanorods in the field of hydrogen production. The HER process follows a Volmer-Heyrovsky mechanism, and the rates of the discharge step and desorption step appear to be comparable during the HER process. The similarity of charged natures of Co and P in the Co_2P nanorods to those of the hydride-acceptor and proton-acceptor in high efficient Ni_2P catalyst, [NiFe] hydrogenase, and its analogues implies that the HER catalytic activity of Co_2P nanorods might be correlated with the charged natures of Co and P.

Keywords

cobalt phosphide; nanorod; electrocatalyst; hydrogen generation

1. Introduction

The solar-driven splitting of water into molecular hydrogen and oxygen is one of the most promising possibilities for simultaneously solving the global energy crisis and current environmental issues.[1-3] Because of the intrinsically slow hydrogen evolution reaction (HER) kinetics of semiconductors, photocathodes must be decorated with HER catalysts for efficient hydrogen production. Though platinum remains the most effective HER catalyst, having been shown to significantly enhance the hydrogen production capability of photocathodes several decades ago,[4, 5] it is a limited resource and expensive, and so its widespread practical application in the field of solar-driven hydrogen production may be limited. There is therefore a demonstrable need for non-precious HER catalysts.

Recently, a variety of new HER catalysts have been reported, including molybdenum sulfide,[6, 7] molybdenum carbide,[8-10] molybdenum nitride,[10] molybdenum boride,[8] tungsten carbide,[11, 12] tungsten carbonitride,[13] first-row transition-metal dichalcogenides,[14, 15] nickel selenide,[16] nickel phosphide,[17] cobalt phosphide (CoP), [18-20] molybdenum phosphide,[21, 22] and etc. The first-row transition-metal dichalcogenides have similar coordination structure as the active centers in efficient hydrogenase,[15] and the charged natures of metal and P in metal phosphides are similar to those of the hydride-acceptor and proton-acceptor in [NiFe] hydrogenase and its analogues ([Ni(PS3*)(CO)]$^{1-}$ and [Ni(PNP)$_2$]$^{2+}$).[23]

Here the HER performance of cobalt phosphide (Co$_2$P) nanorods is introduced. Although their structure and composition are different from all heretofore reported HER catalysts, the Co$_2$P nanorods

2

exhibit efficient and stable HER catalytic activity in both acidic and basic solutions. The overpotential required for a current density of 20 mA/cm^2 (η_{20}) is as small as 167 mV in acidic solution and 171 mV in basic solution. The η_{20} of the Co_2P nanorods lies in the top 10 of the reported values of non-precious HER catalysts. It is worth noting that the four reported η_{20} better than that of the Co_2P nanorods were obtained from the composites of catalysts and nanostructured conductive supports, including Mo_1So_y particles loaded on reduced graphene oxide (Mo_1So_y /rGO),[10] CoP nanoparticles loading on carbon nanotube (CoP/CNT),[18] CoP nanowires loaded on carbon cloth (CoP/CC),[20] and MoS_2 loaded on mesoporous graphene foam (MoS_2/MGF).[24] The nanostructured conductive supports have been well known to improve the electron transport among catalysts and therefore the performance of catalyst.[25] The charged natures of Co and P in the Co_2P nanorods are similar to those of the hydride-acceptor and proton-acceptor in Ni_2P catalyst, [NiFe] hydrogenase, and its analogues. Such similarity might afford the efficient catalytic activity of the Co_2P nanorods.

2. Materials and methods

2.1 Synthesis of Co_2P nanorods. Cobalt acetate tetrahydrate (0.50 g, 2 mmol) was mixed with oleylamine (12 g, 45 mmol) in a 100 mL round-bottom flask. The flask was heated via a heating mantle. Dispersion was obtained by stirring the mixture at 70 °C. The dispersion was then heated to 120 °C and triphenylphosphine (5.246 g, 20 mmol) was added to the mixture. The flask was pumped under vacuum at 120 °C for 30 min to remove water, and then refilled with N_2. The temperature of the

3

heating mantle was increased to 370 °C and maintained at this value for 10 min. The flask was removed from the heating mantle and cooled to room temperature. The black product was isolated and washed by repeated centrifugation/ultrasonication, with hexane as good solvent and ethanol as non-solvent. Finally, the product was dried under vacuum at room temperature.

2.2 Characterization. The morphology of Co_2P nanorods was assessed by transmission electron microscopy (TEM, 200 kV, JEM2100, JEOL) and scanning electron microscopy (SEM, 7001F, JEOL). The energy-dispersive X-ray spectroscopy (EDX) spectrum was recorded using a GENESIS 2000 XM 30T (EDXA) on a JEM2100. For the TEM investigation, the Co_2P nanorods were dispersed in hexane by ultrasonication. The dispersion was dropped onto a carbon-coated copper grid (300-mesh). The copper grid was then dried at 100 ^{o}C for 5 min before the TEM characterization. Powder X-ray diffraction (XRD) patterns were collected using a D8 Advance diffractometer with graphite-monochromated Cu Kα radiation (λ = 1.54178 Å). The X-ray photoelectron spectroscopy (XPS) experiments were carried out on an ESCALAB250Xi System (ThermoFisher) equipped with a monochromatic Al Kα (1486.6 eV) source and a concentric hemispherical energy analyzer. The binding energy C 1s peak from surface adventitious carbon (284.8 eV) was adopted as a reference for the binding energy measurements.

2.3 Electrochemical performance. Co_2P nanorods (15 mg) were dispersed in hexane (0.5 mL) with the aid of an ultrasonic horn (2 mm diameter, 130 W, 60 min). The dispersion (17 μL) was dropped onto a clean Ti foil (0.5 cm^2) and dried naturally. The Ti foil was polished by sandpaper (7000 mesh),

4

and then cleaned by acetone, ethanol, de-ionized water (15 min each) prior to the drop-coating of the Co_2P nanorods. The Co_2P nanorods loaded on the Ti foil were annealed in 5% H_2/N_2 at 450 ^{o}C for 30 min to remove surface ligands.

All electrochemical measurements were carried out with an electrochemical workstation (CHI 614D, CH Instrument) in a three-electrode configuration, with Co_2P (loaded onto Ti foil) as a working electrode, a graphite rod (6 mm diameter) as a counter electrode, and a mercury/mercurous sulfate electrode (MSE) or mercury/mercury oxide electrode (MMO) as a reference electrode. The samples were assembled into a homemade electrochemical cell, with only a defined area (~0.07 cm^2) of the front surface of the sample exposed to solution during the measurements. The counter electrode was separated from working chamber by porous glass frit.

H_2SO_4 aqueous solution (0.5 M) or KOH aqueous solution (1 M) was used for electrochemical measurements. The MSE is used as the reference electrode in H_2SO_4 solution, and the MMO is used in KOH solution. The solutions were purged with high purity H_2 (99.999%) for 30 min prior to electrochemical measurements. The reversible hydrogen evolution potential (RHE) was determined by the open circuit potential of a clean Pt electrode in the solution of interest bubbled with H_2 (99.999%), being -0.694 V vs. MSE for the 0.5 M H_2SO_4 solution and -0.876 V vs. MMO for the 1 M KOH solution. A potential measured with respect to the MSE electrode was therefore referenced to the RHE by adding a value of 0.694 V for the measurements in the 0.5 M H_2SO_4 solution, and a potential measured with respect to the MMO electrode in the KOH solution was referenced to the RHE by

5

adding a value of 0.876 V.

Polarization curves of Co_2P samples were measured at a sweep rate of 5 mV/s in rigorously stirred solution (1600 rpm). The uncompensated cell resistance (R) was determined by current-interrupt method, and the experimental potential was corrected by subtracting ohmic drop (iR), where i is the current corresponding to the experimental potential. The apparent Tafel slope was derived from the iR-corrected polarization curve by fitting experimental data to the equation $\eta = a + b\log j$, where η is the iR-corrected potential, a is the Tafel constant, b is the Tafel slope, and j is the current density. Electrochemical impedance spectroscopy (EIS) measurements were carried out at different potentials in the frequency range of 10^{-2} to 10^6 Hz with 10 mV sinusoidal perturbations and 12 steps per decade in 0.5 M H_2SO_4 solution.

For accelerated degradation investigations, cyclic voltammetric (CV) measurements were carried out with a 50mV/s sweep rate between -0.240 and 0.100 V vs. RHE in the 0.5 M H_2SO_4 solution, and -0.330 and 0.080 V vs. RHE in the 1 M KOH solution, without accounting for uncompensated resistance.

The volume of H_2 during the potentiostatic electrolysis experiment was monitored by volume displacement in a configuration shown in Figure S1 (Electronic Supplementary Information). In this experiment, the backside of the Ti foil was connected to a Cu wire with Ag paste. The Cu wire was threaded to a glass tube (6 mm diameter), and the backside and front side of sample electrode were then sealed with epoxy resin with the exception of an exposed area (~ 0.5 cm^2). A Freescale

6

MPXV7002DP differential pressure transducer was employed to monitor pressure variation in the gas gathering tube, and then the volume of generated H_2 was computed from pressure variation in the gas gathering tube (see details in Electronic Supplementary Information). The current and charge passing the Co_2P nanorods were measured with the electrochemical workstation and the voltage change of the differential pressure transducer was monitored with a digital multimeter (4 1/2 digits). Prior to experiment, the relationship between volume of gathered gas and the variation of output voltage of the differential pressure transducer (i.e., pressure variation in the gas gathering tube) was calibrated by injecting known amounts of air into the gas gathering tube and recording the variation of output voltage of the differential pressure transducer.

3. Results and discussion

Co_2P nanorods were synthesized using low cost precursors at 370 °C. Cobalt acetate and triphenylphosphine were adopted as cobalt source and phosphorus source, respectively, and oleylamine was used as heating media and surface capping agent. The overall structural feature of the resultant Co_2P nanorods was revealed by XRD experiments (Figure 1). The observed well-defined peaks are consistent with the good crystallinity of the products, the peaks matching well those from orthorhombic phase Co_2P (JCPDS No. 32-306, a = 5.6465 Å, b = 6.6099 Å, c = 3.5130 Å).
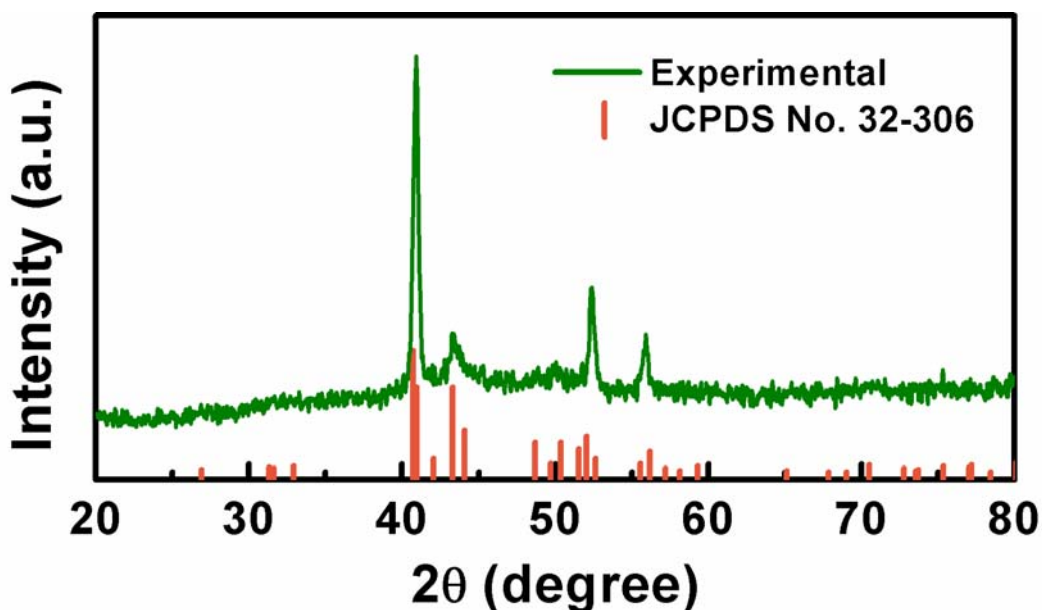
7

Figure 1. Experimental XRD pattern of the Co_2P nanorods.

The morphology and microstructure of the Co_2P nanorods were assessed via TEM. A typical TEM image can be found in Figure 2a. The product has a rod-like morphology, with 9.8 ± 1.3 nm diameter and 110.0 ± 11.8 nm length (Figure S2, Electronic Supplementary Information). The rod-like morphology of the Co_2P was further confirmed by a SEM image (Figure S3, Electronic Supplementary Information). A high resolution TEM (HRTEM) image of the Co_2P nanorods can be found in Figure 2b, in which lattice fringes can be clearly seen. These fringes suggest the good crystallinity of Co_2P, in accordance with that revealed by the XRD experiment. The fast Fourier transform (FFT) pattern of the lattice fringes shows the corresponding diffraction pattern of the Co_2P nanorods (inset of Figure 2b). The pattern can be indexed to the [-210] zone-axis patterns of orthorhombic phase Co_2P ($1/d_{OA} = d_{(121)}$ $= 2.2$ Å, $1/d_{OB} = d_{(002)} = 1.7$ Å, $1/d_{OC} = d_{(-1-21)} = 2.2$ Å, $\angle AOB = \angle BOC = 51°$). The FFT pattern reveals that the Co_2P nanorods grew along the [002] direction. HRTEM images from other nanorods reveal the

8

same growth direction. EDX spectra recorded from nanorods confirm the presence of Co and P in the

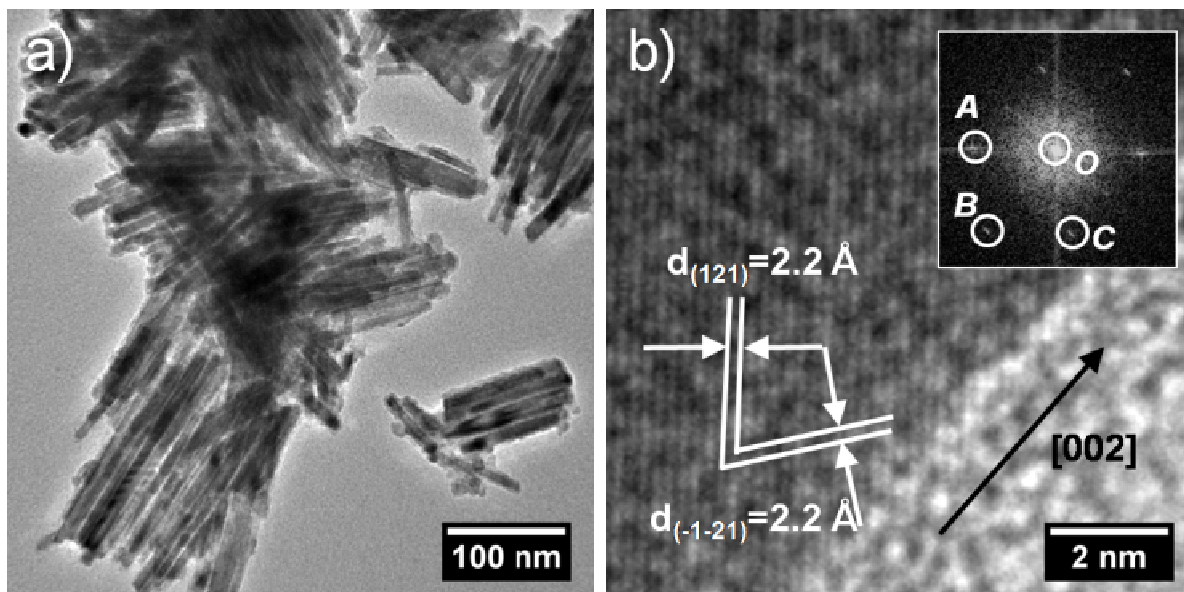nanorods (Figure S4, Electronic Supplementary Information).

Figure 2. (a) TEM and (b) HRTEM images of the Co_2P nanorods.

The chemical states of Co and P on the surface of the Co_2P nanorods were revealed by XPS

experiments. Figure 3 shows the XPS spectra of the Co 2p window and the P 2p window recorded

from the Co_2P nanorods subjected to annealing (450 °C, 5% H_2/N_2, 30 min). Three distinct doublets

can be clearly seen in the XPS spectrum of the Co 2p window (Figure 3a), with Co $2p_{3/2}$ binding

energies at 778.2, 781.7 and 785.6 eV. The peak at 778.2 eV suggests that there are reduced Co species

in Co_2P.[36] These reduced Co species are partially charged ($Co^{\delta+}$, $0 < \delta < 2$), and δ must have a small

value, because the corresponding Co $2p_{3/2}$ binding energy (778.2 eV) is very close to that of metallic

Co (777.9 eV).[26] The P 2p window of the XPS spectrum shows two doublets with peak binding

9

energies at 129.4 and 133.5 eV. The doublet at 129.4 eV suggests the presence of partially negatively

charged P ($P^{\delta-}$, $-1 < \delta < 0$), and the value of δ is likely to be small, because the corresponding energy

(129.4 eV) is close to that of elemental P (130.0 eV).[27] The Co 2p peak observed at 781.7 eV and its

satellite at 785.6 eV can be assigned to Co oxidation state, which could be associated with cobalt

phosphate formed on the surface of the Co_2P nanorods.[28] The presence of cobalt phosphate on the

surface of Co_2P nanorods is also suggested by P 2p peak centered at 133.5 eV and O 1s peak centered

at 531.6 eV (Figure S5, Electronic Supplementary Information), which resemble well those of P and O
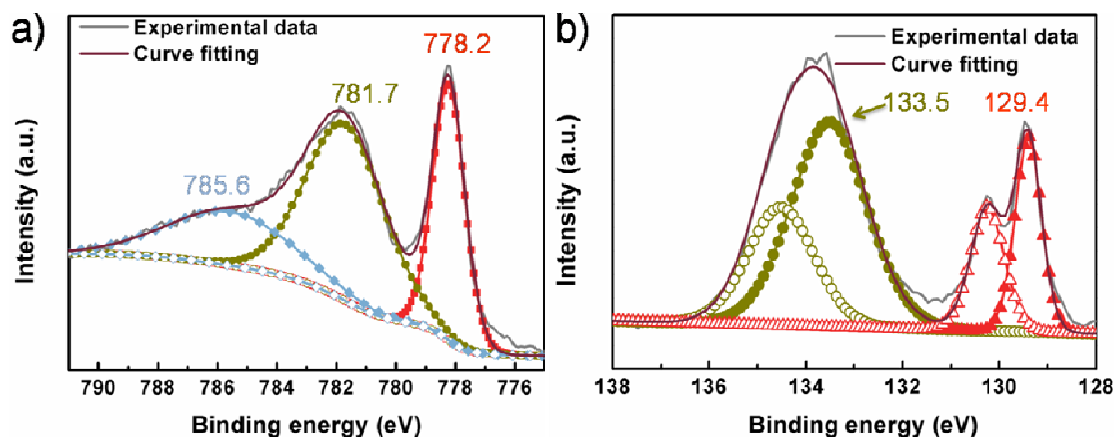
species in cobalt phosphate.[28]

Figure 3. XPS spectra of (a) the Co $2p_{3/2}$ and (b) the P 2p windows.

The HER performance of the Co_2P nanorods was evaluated by polarization curve measurements

(j-V plots). Prior to measurements, The Co_2P nanorods were applied to Ti foils (loading amount ca. 1

mg/cm^2) by drop coating, and annealed at 450 °C in a 5% H_2/N_2 atmosphere for 30 min to remove

surface ligand.[17] The measurements were carried out in a 0.5 M H_2SO_4 solution with a three-

10

electrode configuration (see details in Materials and methods). Figure 4a shows the *j-V* plots of the Co$_2$P nanorods, bare Ti foil, commercial Pt/C (Johnson Matthey, Hispec 3000, 20 wt.%) loaded on a glassy carbon electrode (GCE), and a bare GCE. It was verified that cobalt phosphate can be dissolved in the 0.5 M H$_2$SO$_4$ solution (Figure S6, Electronic Supplementary Information), therefore the cobalt phosphate presented on the surface of the Co$_2$P nanorods would be dissolved and should not affect the catalytic activity of Co$_2$P nanorods during the electrochemistry measurements. It can be seen that the bare Ti foil exhibits negligible current flow in the potential range of -250 to 0 mV vs. RHE, suggesting that the current flow of the Co$_2$P nanorods supported on the Ti foil sample in this potential range is induced by the Co$_2$P nanorods, but not the Ti foil. The onset of current is found at ca. -70 mV vs. RHE for the Co$_2$P nanorods. The η_{20} is 167 mV for the Co$_2$P nanorods, and the overpotential required for a current density of 10 mA/cm^2 (η_{10}) is 134 mV. The η_{20} and η_{10} values of different catalysts are usually compared in order to evaluate their efficiencies, because in photoelectrochemical applications a photocathode produces a current flux of 10-20 mA/cm^2 under 1 sun of AM 1.5 G illumination.[3] The performance of representative HER catalysts is summarized in Table 1. It can be seen that the η_{20} and η_{10} values of the Co$_2$P nanorods in our experiments are only larger than those of CoP nanoparticles,[19] Ni$_2$P nanoparticles,[17] Ni-Mo nanopowders,[29] MoP nanoparticles,[21, 22] CoP/CC,[20] CoP/CNT,[18] Mo$_1$Soy/ rGO [10] and MoS$_2$/ MGF),[24] and smaller than other listed catalysts. Ni-Mo nanopowders degrade rapidly in acidic condition, rendering their exploitation problematic.[29] The conductive CC, CNT, rGO, MGF in CoP/CC, CoP/CNT, Mo$_1$Soy/rGO or MoS$_2$/MGF enhances the

11

HER performance of these composites, in contrast to the Co_2P nanorods in our experiments which are loaded on the Ti foil. This comparison demonstrates that the HER performance of the Co_2P nanorods in our experiments is favorably comparable to most values of recently reported high efficiency non-precious electrocatalysts.
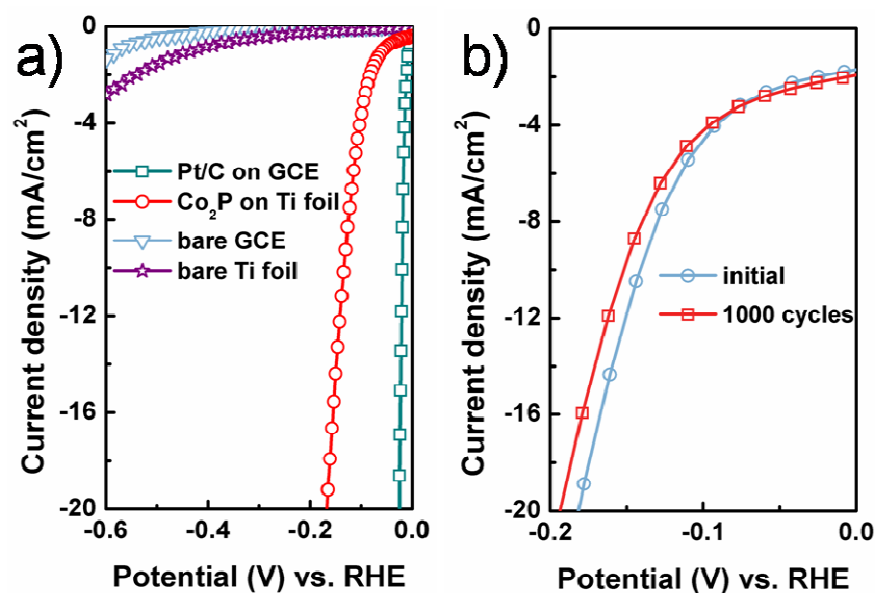

Figure 4. (a) Polarization curves of Pt/C on GCE (loading amount: ~0.285 g/cm^2), Co_2P on Ti foil, bare GCE, and bare Ti foil in 0.5 M H_2SO_4 solution (*iR* corrected). The bare Ti foil was subjected to the same annealing treatment as Co_2P on Ti foil sample prior to the measurement. (b) Polarization curves of Co_2P on Ti foil in 0.5 M H_2SO_4 at different CV sweeps (without *iR* correction).

12

Table 1. Summary of the HER performance of representative catalysts.

Catalyst	Substrate	Mass density (mg/cm^2)	η_{onset}[a] (mV)	η_{10} (mV)	η_{20} (mV)	Tafel slope (mV/dec)	J_0[b] (mA/cm^2)	Electrolyte
Ni_2P[17]	Ti foil	1		117	130	$46_{\eta=25-125}$ $81_{\eta=150-200}$	3.3×10^{-3}	$0.50M\ H_2SO_4$
CoP[30]	Ti foil	2			85	50	0.14	$0.50\ M\ H_2SO_4$
CoP[20]	carbon cloth	0.92	38	67	100	51	0.288	$0.50\ M\ H_2SO_4$
CoP/CNT[18]	GCE	0.285	40	122	160	54	0.13	$0.50\ M\ H_2SO_4$
MoP[22]	GCE	0.36	40	125	151	54	0.086	$0.50\ M\ H_2SO_4$
MoP[21]	GCE	0.86	50	135	167	54	0.034	$0.50\ M\ H_2SO_4$
Ni-Mo nanopowder[29]	Ti foil	1			70			2 M NaOH
Ni-Mo nanopowder[29]	Ti foil	3			80			$0.5\ M\ H_2SO_4$
Ni-Mo nanopowder[29]	Ti foil	1		79	107			1 M NaOH
Bulk Mo_2C[8]	carbon paste electrode	1.4	$\geqq 100$	208	224	$56_{\eta=100-220}$	1.3×10^{-3}	$0.50\ M\ H_2SO_4$
Bulk MoB[8]	carbon paste electrode	2.5	$\geqq 100$	212	227	$55_{\eta=140-210}$	1.4×10^{-3}	$0.50\ M\ H_2SO_4$
Mo_2C/CNT[9]	carbon paper	2	63	149		55.2	1.4×10^{-2}	$0.1\ M\ HClO_4$
Fe-WCN[13]	RRDE	0.4	100	220		47.1		H_2SO_4 (pH 1) + Na_2SO_4 (0.5 M)
Mo_1Soy[10]	carbon paper	1.4		177		66.4	1.3×10^{-2}	$0.1\ M\ HClO_4$
Mo_1Soy-RGO[10]	carbon paper	0.47		109		62.7	3.7×10^{-2}	$0.1\ M\ HClO_4$
Mo_2C/C[10]	carbon paper	2		311		87.6	8.1×10^{-3}	$0.1\ M\ HClO_4$
$Co_{0.6}Mo_{1.4}N_2$[31]	GCE	0.243		202	267		2.3×10^{-4}	$0.1M\ HClO_4$
MoS_3(33%)/MWCNT-NC[32]	silver electrode	0.255	130	206	226	$40_{\eta=135-174}$	1.35×10^{-4}	$1\ M\ H_2SO_4$
Core-shell MoO_3-MoS_2 nanowires[33]	FTO		150-200	254	272	$50-60_{\eta=200}$		$0.5\ M\ H_2SO_4$
Defect-rich MoS_2 nanosheets[34]	GCE	0.285	120	190	214	$50_{\eta=120-180}$	8.91×10^{-3}	$0.5\ M\ H_2SO_4$
MoS_2@Au[35]	Au electrode	0.00103	90	226		69	9.3×10^{-3}	$0.5\ M\ H_2SO_4$
amorphous MoS_3-CV[7]	GCE			211	229	$40_{\eta=170-200}$	1.3×10^{-4}	$1\ M\ H_2SO_4$
MoS_2/RGO hybrid[25]	GCE	0.285	100	154	176	41		$0.5M\ H_2SO_4$
MoS_2/MGF[24]	GCE	0.21	100	146	159	$42_{\eta=90-120}$		$0.5\ M\ H_2SO_4$
MoS_2/CNTs[36]	glass carbon disk	0.136	90	184	230	44.6		$0.5\ M\ H_2SO_4$
Cu_2MoS_4[37]	GCE	0.0425	135	321		95		pH 0 H_2SO_4
WS_2/RGO[38]	GCE	0.4	150-200	265	292	58		$0.5M\ H_2SO_4$
WS_2 nanosheets[39]	GCE	0.0001-0.0002 or ca. one continuous layer	80-100	233	275	55		$0.5\ M\ H_2SO_4$
WS_2 nanosheets[40]	GCE	0.285	60	151	177	72	2.5×10^{-3}	$1\ M\ H_2SO_4$
Cobalt-sulfide catalyst[41]	FTO		43	165	227	93		1.0 M pH 7 PBS
$NiWS_x$[42]	FTO		165	373	430	$96_{\eta=120-150}$	$10^{-2.66}$	pH 7 PBS
$CoWS_x$[42]	FTO		95	271	311	$78_{\eta=120-150}$	$10^{-2.25}$	pH 7 PBS
$CoMoS_x$[42]	FTO		75	241	282	$85_{\eta=120-150}$	$10^{-2.89}$	pH 7 PBS
FeS_2[15]	GCE			192.6		62.5	7×10^{-4}	$0.5\ M\ H_2SO_4$
$FeSe_2$[15]	GCE					65.3	3.5×10^{-4}	$0.5\ M\ H_2SO_4$
$Fe_{0.43}Co_{0.57}S_2$[15]	GCE			264		55.9	1.3×10^{-3}	$0.5\ M\ H_2SO_4$
CoS_2[15]	GCE			232		44.6	6.5×10^{-5}	$0.5\ M\ H_2SO_4$
$CoSe_2$[15]	GCE	0.037	45	231		42.4	6.5×10^{-5}	$0.5\ M\ H_2SO_4$
$Co_{0.56}Ni_{0.44}Se_2$[15]	GCE			250		49.7	6.3×10^{-5}	$0.5\ M\ H_2SO_4$
$Co_{0.32}Ni_{0.68}S_2$[15]	GCE					66.8	3.0×10^{-4}	$0.5\ M\ H_2SO_4$
NiS_2[15]	GCE					41.6	1.4×10^{-4}	$0.5\ M\ H_2SO_4$

13

NiSe$_2$[15]	GCE	250	56.9	5.7×10^{-4}	0.5 M H$_2$SO$_4$

[a] η_{onset}: overpotential for the onset of reductive current

[b] J$_0$: exchange current density

High durability is of importance for a good electrocatalyst. The stability of the Co$_2$P nanorods was evaluated by cyclic voltammetry (CV) sweeps between -0.240 and 0.100 V vs. RHE in the 0.5 M H$_2$SO$_4$ solution. The corresponding *j-V* curves of the CV sweeps (without *iR* correction) are shown in Figure 4b. After 1000 CV sweeps the η_{20} increases from 181 mV to 194 mV, the increase of the η_{20} being smaller than 15 mV. The current density at 0 V vs. RHE in CV sweeps (2 mA/cm^2, Figure 4b) is larger than that in Figure 4a ($\sim$ 0 mA/cm^2). It is apparent that the larger current density is correlated with the faster scan rate (50 mV/s) in CV sweeps, implying that the current density at 0 V vs. RHE in CV sweeps could be associated with the capacitive process on the surface of the catalyst. In addition, current density exhibits only ca. 10% decrease after 12 h potentiostatic electrolysis (Figure S7, Electronic Supplementary Information). The CV sweeps and potentiostatic electrolysis experiment suggest the HER stability of the Co$_2$P nanorods in acidic solution.

Thus far, only rare excellent catalysts (e.g. Pt and Mo$_2$C)[8] have been shown to perform reliably in both acidic and basic solution. For this reason, the HER performance of the Co$_2$P nanorods in basic solution (KOH, 1 M) was also evaluated. The corresponding results are shown in Figure S8 (Electronic Supplementary Information), with a η_{20} value of 171 mV (*iR* corrected). After 1000 CV sweeps between -0.330 and 0.080 V vs. RHE, the η_{20} increases from 217 mV to 229 mV (without *iR* correction). The relatively small increase of the η_{20} (12 mV) and a potentiostatic electrolysis

14

experiment (Figure S8c, Electronic Supplementary Information) shows the stability of the Co_2P nanorods in the basic solution. These experiments demonstrate that the Co_2P nanorods can function efficiently and stably under the basic condition as well. It has been reported that the η_{20} of Ni_2P nanoparticles in basic solution (KOH, 1 M) is 205 mV, and the HER performance declined rapidly on cycling.[17] The reason for the different stabilities of the Co_2P nanorods and the Ni_2P nanoparticles in basic solution remains unknown, but the different crystal structures (orthorhombic Co_2P and hexagonal Ni_2P) are likely to be an important factor.

The faradaic efficiency of the Co_2P nanorods during H_2 evolution was probed by comparing the volume of generated gas and quantity of charges passing the Co_2P nanorods while a potentiostatic electrolysis measurement was carried out. The volume of generated gas was monitored by the water displacement method. Figure 5 shows the comparison of the theoretical volume of hydrogen and the experimentally measured volume of hydrogen. 10 C of charge pass through the cathode ($\sim$0.5 cm^2) in 1310 s, 1.25 mL of H_2 should be produced according to the theoretical computation. In the experiment, the volume of generated H_2 was measured to be 1.18 mL, very close to the theoretical value. In addition, the faradaic yield of H_2 production is nearly 100% over the time scale of the measurement (Figure 5).
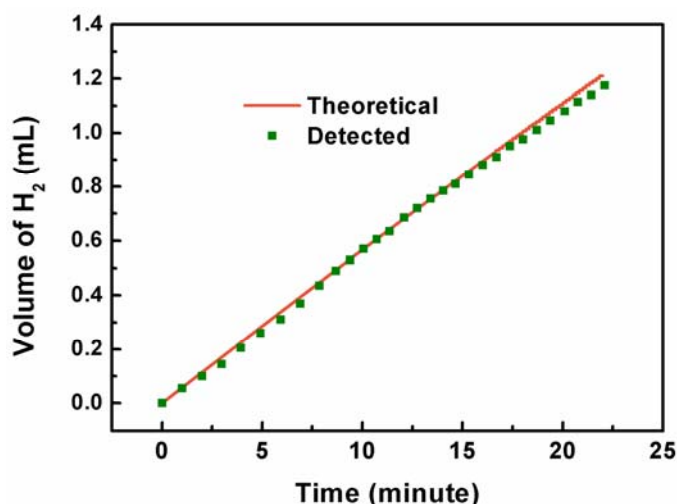
15

Figure 5. Current efficiency for HER under potentiostatic electrolysis (applied potential: -150 mV vs. RHE).

To obtain insight into the HER process and mechanism with the Co_2P nanorods, electrochemical impedance spectroscopy (EIS) investigations were carried out. The EIS experiments were carried out at different applied potentials, the results being shown in Nyquist plots in Figure 6. The EIS spectra display two semicircles. The semicircles at high frequencies (shown more clearly in Figure 6b) can be related to the contact between the catalyst (Co_2P) and the catalyst support (Ti foil), while those at low frequencies correspond to the kinetics of the HER process on the surface of the catalyst.

The diameters of the semicircles at low frequencies are potential-dependent, decreasing with increasing applied potential. This is qualitatively in accordance with faster HER kinetics occurring at higher overpotential. The kinetics of electrochemical reaction at an electrode's surface is usually assessed by charge transfer resistance (R_{ct}), with a smaller R_{ct} value corresponding to faster kinetics. R_{ct} can be deduced from EIS spectra by data fitting, in the present case using the equivalent circuit shown in Figure S9 (Electronic Supplementary Information). The results are listed in Table S1

16

(Electronic Supplementary Information). The high frequency constant phase element (CPE$_1$) and resistance element (R$_1$) are nearly potential-independent (Figures S10a and S10b, Electronic Supplementary Information). In contrast, R$_{ct}$ is potential-dependent (Figure S10d, Electronic Supplementary Information) whereas the low frequency constant phase element (CPE$_{dl}$) is nearly potential-independent (Figure S10c, Electronic Supplementary Information). The invariant CPE$_{dl}$ value suggests that the active surface area of the catalyst is maintained at different applied potentials, consistent with a high durability of the catalyst.
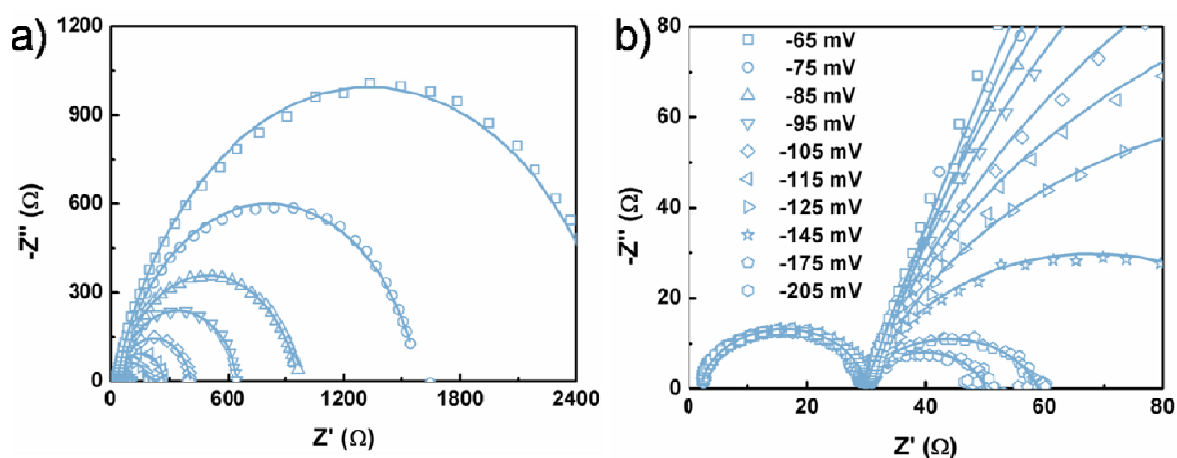
Figure 6. Nyquist plots of EIS responses of the Co$_2$P nanorods at different applied potentials in 0.5 M H$_2$SO$_4$ solution: (a) the overall spectra, and (b) data near the high frequency region. The scatters show the experimental data, and lines show the results of fitting to the equivalent circuit in Figure S9.

In general, classic two-electron-reaction models suggest that the HER process proceeds in two steps: a discharge step (Volmer reaction: H$_3$O$^+$ + e$^-$ → H$_{ads}$ + H$_2$O) followed by a desorption step (Heyrovsky reaction: H$_{ads}$ + H$_3$O$^+$ + e$^-$ → H$_2$ + H$_2$O), or a discharge step followed by a recombination step (Tafel reaction: H$_{ads}$ + H$_{ads}$ → H$_2$), where H$_{ads}$ represents an H atom absorbed at the active site of the catalyst. The rate-limiting step can be identified by the Tafel analysis of the catalyst, with a Tafel

17

slope of 116, 38, or 29 mV/decade assigning the rate-determining step in the HER process to Volmer, Heyrovsky, or Tafel reaction. The polarization curve (Figure 4a) is presented in a Tafel plot in Figure 7a, and the apparent Tafel slope obtained by fitting the linear portion of the Tafel plot to the Tafel equation. The apparent Tafel slope of Co_2P fitted from the polarization curve is 71.0 mV/decade. The apparent Tafel slope extracted from the polarization curve will be higher than the true value, if electron transport in the catalyst is sufficiently slow. For example, it has been shown that different loading amounts of MoS_x on GCE result in different Tafel slopes,[43] and the introduction of reduced graphene oxide to MoS_2 can markedly reduce the Tafel slope.[25] Hu and Vrubel et al. demonstrated that the contribution of the electron transport process in the catalyst to the Tafel slope can be eliminated if the Tafel slope is derived from EIS data.[43] The $\log(1/R_{ct})$-η plot of the Co_2P nanorods is shown in Figure 7b, showing a Tafel slope of 51.7 mV/decade.

The Tafel slope of 51.7 mV/decade lies between 38 and 116 mV/decade, suggesting that a Volmer-Heyrovsky mechanism might be responsible for the HER process,[10] and that the rates of the discharge step and the desorption step might be comparable during the HER process.[16] The Tafel slope fitted from the polarization curve is larger than that obtained from R_{ct}, suggesting that electron transport resistance in the catalyst may be well comparable to the charge transfer resistance at the catalyst/electrolyte interface. The apparent Tafel slope would thereby be reduced and, accordingly, the HER performance could be further improved by reducing the electron transport resistance in the catalyst, for example via the introduction of conductive graphene.[25] On the other hand, the turnover

18

frequencies (TOFs) of the HER were estimated according to the number active sites determined by CV sweep. [7] In this approach the total number of active sites is the upper limit value. Figure S11 (Electronic Supplementary Information) shows the plot of TOFs versus the applied potentials in the 0.5 M H_2SO_4 solution. The Co_2P nanorods show a TOF of 0.725 S^{-1} at -143 mV vs. RHE. This value is larger than that of CoP/CC (~ -75 mV vs. RHE),[20] and smaller than that of MoS_3 deposited on GCE (~ -220 mV vs. RHE). [7]
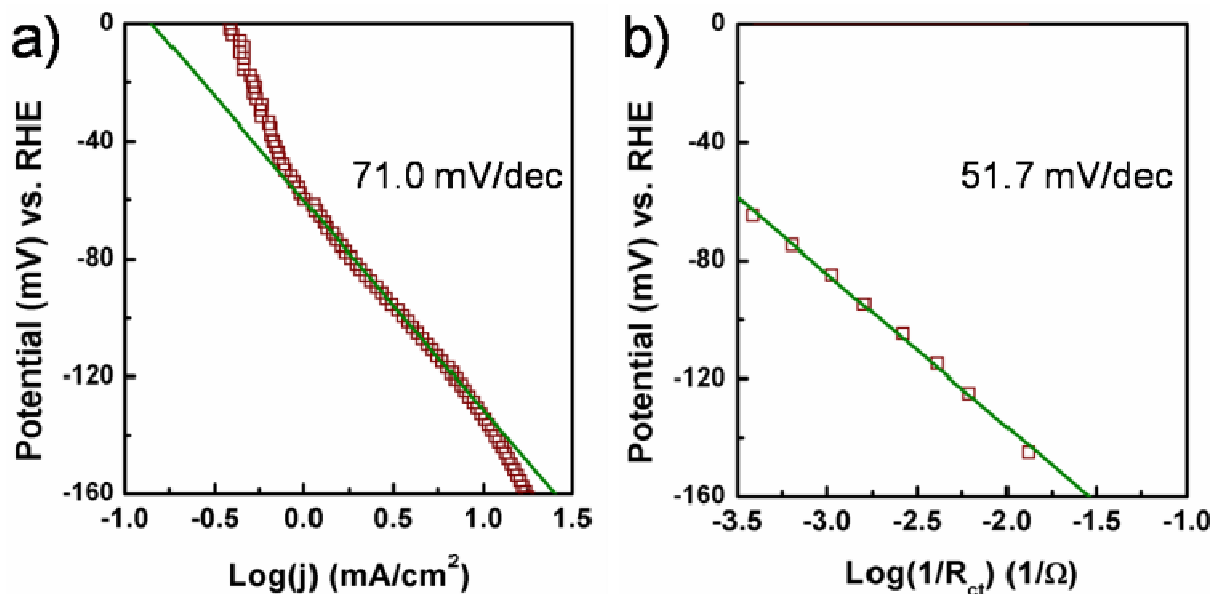
Figure 7. (a) Apparent Tafel slope fitted from polarization data measured in 0.5 M H_2SO_4 solution, and (b) Tafel slope fitted from EIS data measured in 0.5 M H_2SO_4 solution. Scatters show experimental data and the solid lines show the corresponding fitting.

The HER catalytic activity of the Co_2P nanorods might be correlated with the unique charged natures of Co and P species. The kinetics of HER in [NiFe] hydrogenase and its analogues ($[Ni(PS3*)(CO)]^{1-}$ and $[Ni(PNP)_2]^{2+}$) have been assessed via density functional theory simulation.[23] It was revealed that the efficient hydrogenase and its analogues have both proton acceptor and hydride

19

acceptor sites. The proton acceptor site is the nonmetal site having a small negative charge to trap protons (e.g., O of Glu23 in hydrogenase, -0.44 e; S in Ni(PS3*)(CO)]$^{1-}$, -0.4 e; N in [Ni(PNP)$_2$]$^{2+}$, -0.34 e). The hydride acceptor site (Ni in hydrogenase, Ni(PS3*)(CO)]$^{1-}$, and [Ni(PNP)$_2$]$^{2+}$) is the isolated metal atom providing moderate bonding to hydrogen, and the hydride acceptor site has a slightly positive charge, suggested by the calculated total electron density of hydrogenase, Ni(PS3*)(CO)]$^{1-}$, and [Ni(PNP)$_2$]$^{2+}$. The proton acceptor and hydride acceptor sites work cooperatively, resulting in high HER catalytic activities. Ni$_2$P(001) also has proton acceptor sites (P) and hydride acceptor sites (Ni), and it has been predicted[23] and then proved[17] to be highly active HER catalyst. The hydride acceptor (Ni) and proton acceptor (P) in Ni$_2$P has small positive and negative charges, respectively, suggested by the fact that the peak binding energies of Ni (853.5 eV) and P (129.5 eV) in Ni$_2$P are very close to those of the corresponding zero valence species (852.8 eV for Ni and 130.0 eV for P).[44] It has been revealed that Co and P in Co$_2$P also have a small positive and negative charge (Figure 3 and corresponding discussion). The charged natures of Co and P in Co$_2$P are therefore similar to those of hydride acceptor and proton acceptor in Ni$_2$P, [NiFe] hydrogenase, [Ni(PS3*)(CO)]$^{1-}$, and [Ni(PNP)$_2$]$^{2+}$), respectively. The similarity in charged natures implies that similar catalytic mechanism might work in the Co$_2$P nanorods as Ni$_2$P, [NiFe] hydrogenase, [Ni(PS3*)(CO)]$^{1-}$, and [Ni(PNP)$_2$]$^{2+}$), resulting to high HER catalytic activity reported here.

20

4. Conclusions

In conclusion, Co_2P nanorods were demonstrated as a new efficient HER electrocatalyst. The HER performance of the Co_2P nanorods is comparable to those of high efficiently non-precious electrocatalysts. Accelerated degradation and potentiostatic electrolysis experiments have demonstrated the stability of the Co_2P nanorods in acidic and basic solution during the HER process. The faradaic yield of H_2 production is nearly 100%. The HER process was found to follow a Volmer-Heyrovsky mechanism, and the rates of the discharge and desorption step appear to be comparable during the HER process. The HER performance could be further improved by the introduction of conductive species. Studies directed toward this goal are currently underway.

21

References

[1]   S. S. Mao, X. B. Chen, Inter. J. Energ. Res., 31 (2007) 619-636.

[2]   T. R. Cook, D. K. Dogutan, S. Y. Reece, Y. Surendranath, T. S. Teets, D. G. Nocera, Chem. Rev., 110 (2010) 6474-6502.

[3]   M. G. Walter, E. L. Warren, J. R. McKone, S. W. Boettcher, Q. X. Mi, E. A. Santori, N. S. Lewis, Chem. Rev., 110 (2010) 6446-6473.

[4]   M. Szklarczyk, J. O. M. Bockris, Appl. Phys. Lett., 42 (1983) 1035-1036.

[5]   R. N. Dominey, N. S. Lewis, J. A. Bruce, D. C. Bookbinder, M. S. Wrighton, J Am Chem Soc, 104 (1982) 467-482.

[6]   B. Hinnemann, P. G. Moses, J. Bonde, K. P. Jørgensen, J. H. Nielsen, S. Horch, I. Chorkendorff, J. K. Nørskov, J Am Chem Soc, 127 (2005) 5308-5309.

[7]   D. Merki, S. Fierro, H. Vrubel, X. L. Hu, Chem. Sci., 2 (2011) 1262-1267.

[8]   H. Vrubel, X. L. Hu, Angew. Chem. Int. Ed., 51 (2012) 12703-12706.

[9]   W. F. Chen, C. H. Wang, K. Sasaki, N. Marinkovic, W. Xu, J. T. Muckerman, Y. Zhu, R. R. Adzic, Energ. Environ. Sci., 6 (2013) 943-951.

[10]   W. F. Chen, S. Iyer, S. Iyer, K. Sasaki, C. H. Wang, Y. M. Zhu, J. T. Muckerman, E. Fujita, Energ. Environ. Sci., 6 (2013) 1818-1826.

22

[11]   F. Harnisch, G. Sievers, U. Schröder, Appl. Catal. B- Environ., 89 (2009) 455-458.

[12]   S. Wirth, F. Harnisch, M. Weinmann, U. Schröder, Appl. Catal. B- Environ., 126 (2012) 225-

230.

[13]   Y. Zhao, K. Kamiya, K. Hashimoto, S. Nakanishi, Angew. Chem. Int. Ed., 52 (2013) 1-5.

[14]   A. Ivanovskaya, N. Singh, R. F. Liu, H. Kreutzer, J. Baltrusaitis, T. V. Nguyen, H. Metiu, E.

McFarland, Langmuir, 29 (2013) 480-492.

[15]   D. S. Kong, J. J. Cha, H. T. Wang, H. R. Lee, Y. Cui, Energ. Environ. Sci., 6 (2013) 3553-

3558.

[16]   M. R. Gao, Z. Y. Lin, T. T. Zhuang, J. Jiang, Y. F. Xu, Y. R. Zheng, S. H. Yu, J. Mater. Chem.,

22 (2012) 13662-13668.

[17]   E. J. Popczun, J. R. McKone, C. G. Read, A. J. Biacchi, A. M. Wiltrout, N. S. Lewis, R. E.

Schaak, J Am Chem Soc, 135 (2013) 9267-9270.

[18]   Q. Liu, J. Q. Tian, W. Cui, P. Jiang, N. Y. Cheng, A. M. Asiri, X. P. Sun, Angew. Chem. Inter.

Ed., 53 (2014) 6710-6714.

[19]   E. J. Popczun, C. G. Read, C. W. Roske, N. S. Lewis, R. E. Schaak, Angew. Chem. Inter. Ed.,

53 (2014) 5427-5430.

[20]   J. Q. Tian, Q. Liu, A. M. Asiri, X. P. Sun, J Am Chem Soc, 136 (2014) 7587-7590.

[21]   P. Xiao, M. A. Sk, L. Thia, X. M. Ge, R. J. Lim, J. Y. Wang, K. H. Lim, X. Wang, Energy

Environ. Sci., 7 (2014).

23

[22]   Z. C. Xing, Q. Liu, A. M. Asiri, X. P. Sun, Adv. Mater. , DOI:10.1002/adma.201401692

(2014).

[23]   P. Liu, J. A. Rodriguez, J Am Chem Soc, 127 (2005) 14871-14878.

[24]   L. Liao, J. Zhu, X. J. Bian, L. N. Zhu, M. D. Scanlon, H. H. Girault, B. H. Liu, Adv. Funct.

Mater., 23 (2013) 5326-5333.

[25]   Y. Li, H. Wang, L. Xie, Y. Liang, G. Hong, H. Dai, J Am Chem Soc, 133 (2011) 7296-7299.

[26]   V. V. Nemoshalenko, V. V. Didyk, V. P. Krivitskii, A. I. Senekevich, Zh. Neorg. Khimii, 28

(1983) 2182-2192.

[27]   V. I. Nefedov, Y. V. Salyn, E. P. Domashevskaya, Y. A. Ugai, V. A. Terekhov, J. Electron

Spectrosc. Relat. Phenom., 6 (1975) 231-238.

[28]   S. Cobo, J. Heidkamp, P. Jacques, J. Fize, V. Fourmond, L. Guetaz, B. Jousselme, V. Ivanova,

H. Dau, S. Palacin, M. Fontecave, V. Artero, Nat. Mater., 11 (2012) 802-807.

[29]   J. R. McKone, B. F. Sadtler, C. A. Werlang, N. S. Lewis, H. B. Gray, ACS Catal., 3 (2013)

166-169.

[30]   E. J. Popczun, C. G. Read, C. W. Roske, N. S. Lewis, R. E. Schaak, Angew. Chem. Inter. Ed.,

53 (2014) 5427-5430.

[31]   B. F. Cao, C. M. Veith, J. C. Neuefeind, R. R. Adzic, P. G. Khalifah, J Am Chem Soc, 135

(2013) 19186-19192.

[32]   T. W. Lin, C. J. Liu, J. Y. Lin, Appl. Catal. B- Environ., 134-135 (2013) 75-82.

24

[33]   Z. Chen, D. Cummins, B. N. Reinecke, E. Clark, M. K. Sunkara, T. F. Jaramillo, Nano. Lett.,

11 (2011) 4168-4175.

[34]   J. Xie, H. Zhang, S. Li, R. Wang, X. Sun, M. Zhou, J. Zhou, X. W. Lou, Y. Xie, Adv. Mater.,

25 (2013) 5807-5813.

[35]   T. Y. Wang, L. Liu, Z. W. Zhu, P. Papakonstantinou, J. B. Hu, M. Li, Energy Environ. Sci., 6

(2013) 625-633.

[36]   Y. Yan, X. Ge, Z. Liu, J. Y. Wang, J. M. Lee, X. Wang, Nanoscale, 5 (2013) 7768-7771.

[37]   P. D. Tran, M. Nguyen, S. S. Pramana, A. Bhattacharjee, S. Y. Chiam, J. Fize, M. J. Field, V.

Artero, L. H. Wong, J. Loo, J. Barber, Energ. Environ. Sci., 5 (2012) 8912-8916.

[38]   J. Yang, D. Voiry, S. J. Ahn, D. Kang, A. Y. Kim, M. Chhowalla, H. S. Shin, Angew. Chem.

Int. Ed., 52 (2013) 13751-13754.

[39]   D. Voiry, H. Yamaguchi, J. Li, R. Silva, D. C. Alves, T. Fujita, M. Chen, T. Asefa, V. B.

Shenoy, G. Eda, M. Chhowalla, Nat. Mater., 12 (2013) 850-855.

[40]   Z. Z. Wu, B. Z. Fang, B. Arman, A. K. Sun, D. P. Wilkinson, D. Z. Wang, Appl. Catal. B-

Environ., 125 (2012) 59-66.

[41]   Y. Sun, C. Liu, D. C. Grauer, J. Yano, J. R. Long, P. Yang, C. J. Chang, J Am Chem Soc, 135

(2013) 17699-17702.

[42]   P. D. Tran, S. Y. Chiam, P. P. Boix, Y. Ren, S. S. Pramana, J. Fize, V. Artero, J. Barber, Energ.

Environ. Sci., 6 (2013) 2452-2459.

25

[43]   H. Vrubel, T. Moehl, M. Gratzel, X. L. Hu, Chem. Commun. , 49 (2013) 8985-8987.

[44]   S. J. Sawhill, K. A. Layman, D. R. Van Wyk, M. H. Engelhard, C. Wang, M. E. Bussell, J.

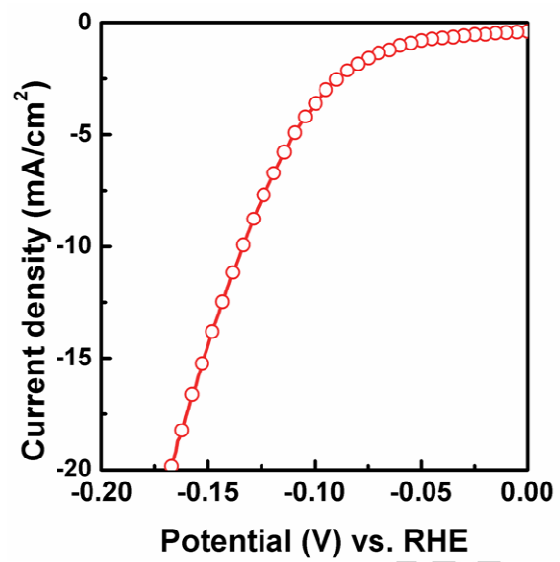Catal., 231 (2005) 300-313.
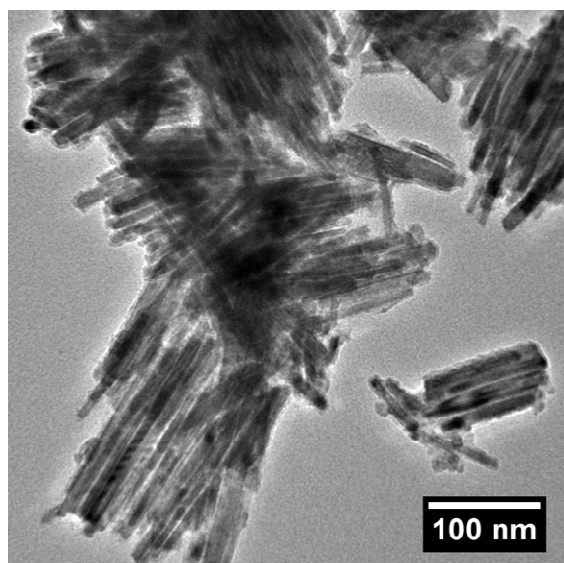
26

Research highlight

A convenient method is used to fabricate cobalt phosphide (Co_2P) nanorods.

Co_2P nanorods exhibit efficient electrocatalytic activity in hydrogen evolution reaction.

Co_2P nanorods work stably in both acidic and basic solutions.

Graphical abstract